Supporting Information for

Transition from Schottky to Ohmic Contacts in 2D Ge/GaAs Heterostructure with High Tunneling Probability

Yang Shen[1,2,*], Jianfeng Zhu[1], Qihao Zhang[1], Hua Zhu[1], Qianglong Fang[1,3],

Xiaodong Yang[4] and Baolin Wang[5]

[1]*Institute of Optical and Electronic Technology, China Jiliang University, Hangzhou 310018, P. R. China*

[2]*School of Materials Science and Engineering, Zhejiang University, Hangzhou 310027, P. R. China*

[3]*School of Physics, Southeast University, Nanjing 211189, P. R. China*

[4]*Key Laboratory of Ecophysics and Department of Physics, Shihezi University, Xinjiang 832003, P. R. China*

[5]*College of Physical Science and Technology, Nanjing Normal University, Nanjing 210023, P. R. China*

[*]Correspondence and requests for materials should be addressed to Y. Shen (yshen@cjlu.edu.cn).

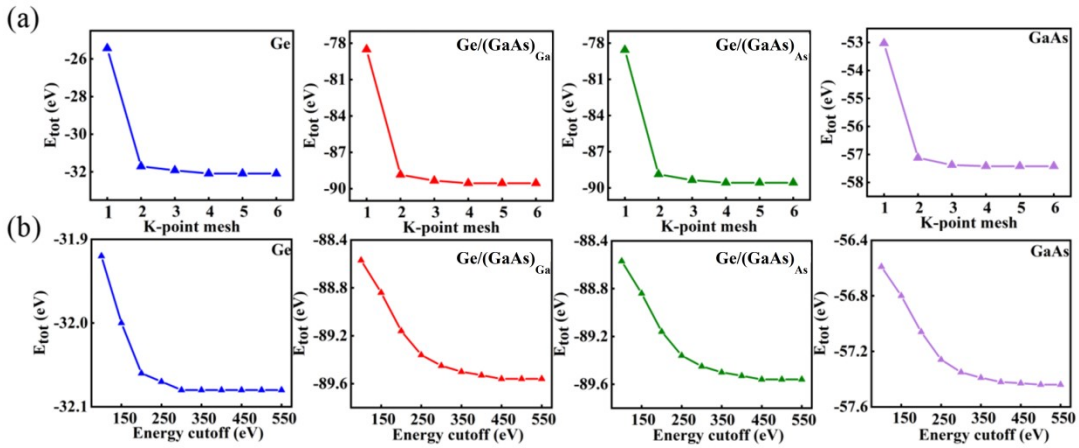

Fig. S1 The total energies (E_{tot}) of Germanene, GaAs monolayer, Ge/(GaAs)$_{Ga}$ heterostructure, and Ge/(GaAs)$_{As}$ heterostructure with different k-point mesh (a) and energy cutoff (b).

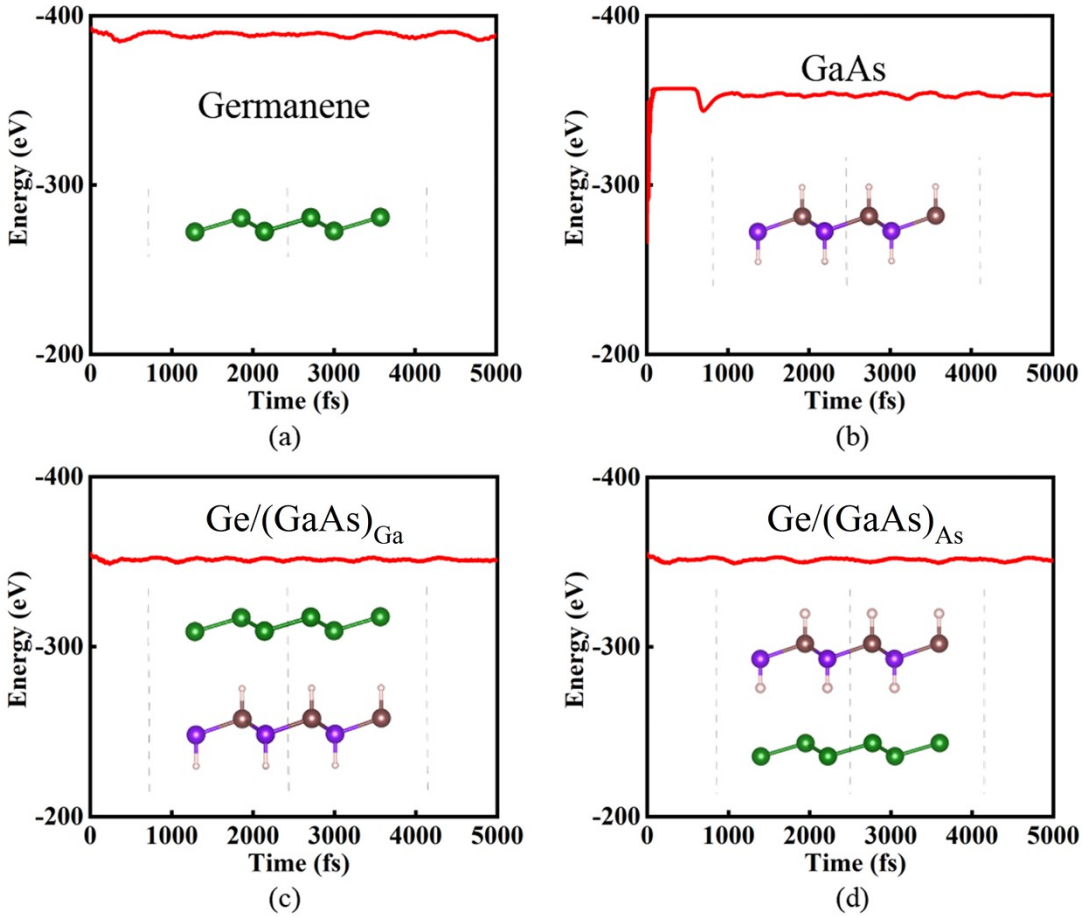

Fig. S2 The most energetically favorable stacking configuration of (a) Germanene monolayer, (b) GaAs monolayer, (c) Ge/(GaAs)$_{Ga}$ heterostructure, (d) Ge/(GaAs)$_{As}$ heterostructure.

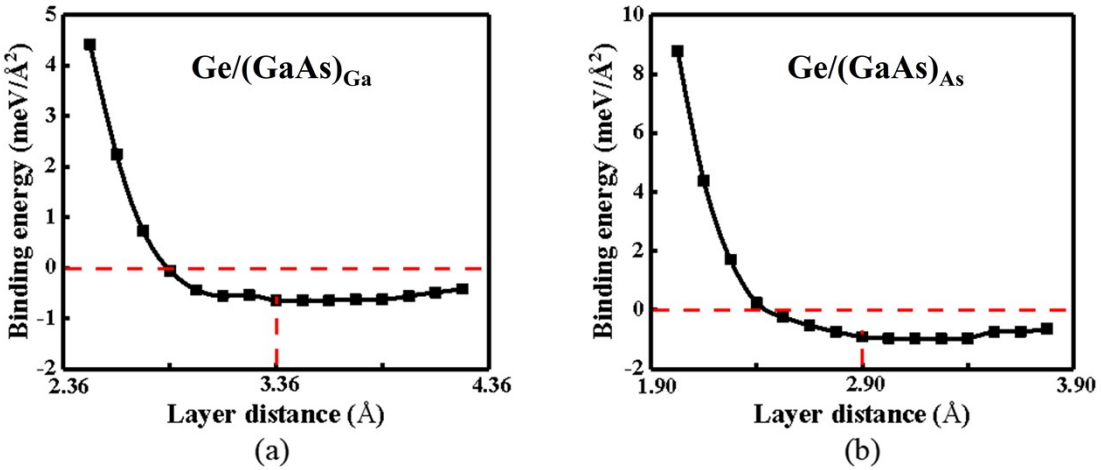

Fig. S3 The binding energies for Ge/GaAs heterostructures under different layer distance (a) $Ge/(GaAs)_{Ga}$ heterostructure, (b) $Ge/(GaAs)_{As}$ heterostructure.

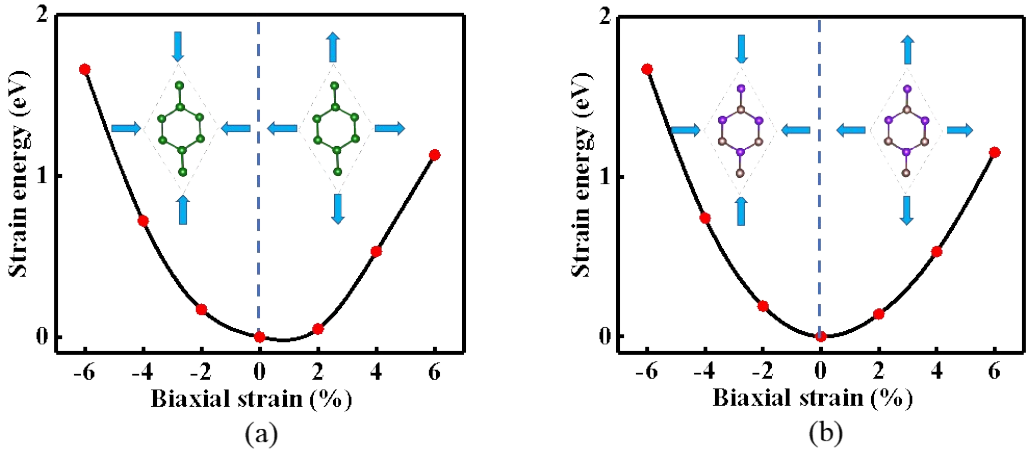

Fig. S4 The strain energies for Ge/GaAs heterostructures under different biaxial strain (a) $Ge/(GaAs)_{Ga}$ heterostructure, (b) $Ge/(GaAs)_{As}$ heterostructure.

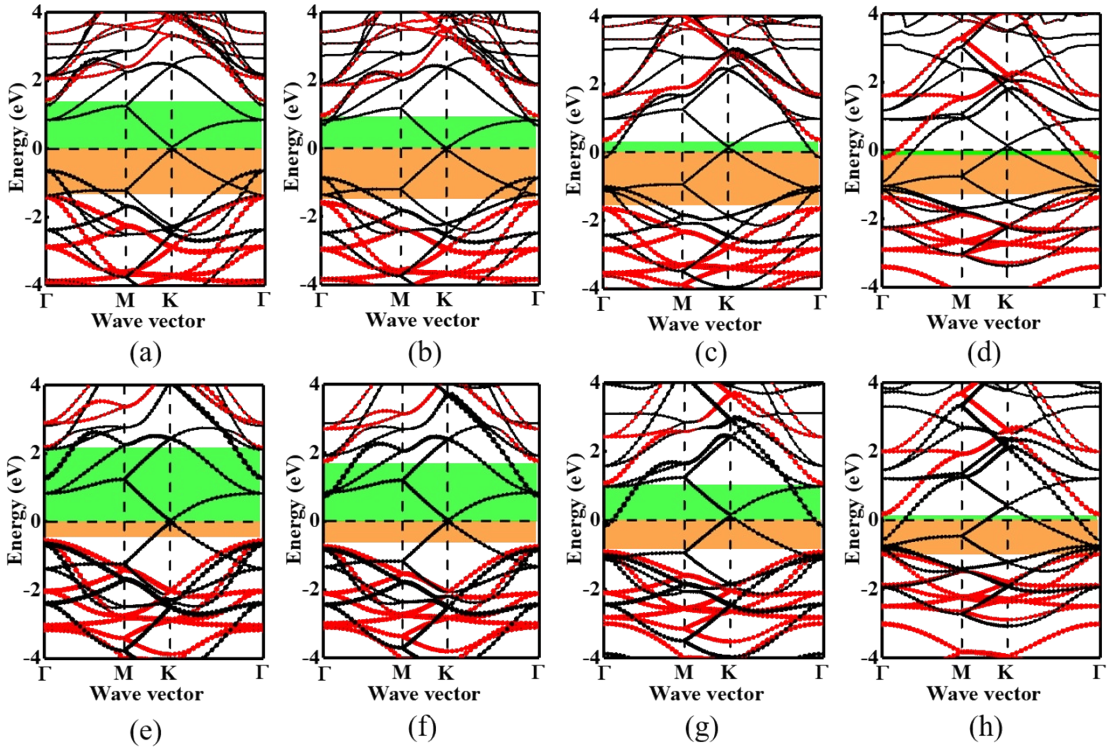

Fig. S5 The band structure of Ge/$(GaAs)_{Ga}$ under (a) -2%, (b)0%, (c)4%, (d)12%, strain, of Ge/$(GaAs)_{As}$ under (e) -2%, (f)0%, (g)4%, (h)12% strain. The light green and light brown areas indicate the Φ_e and Φ_h, respectively.

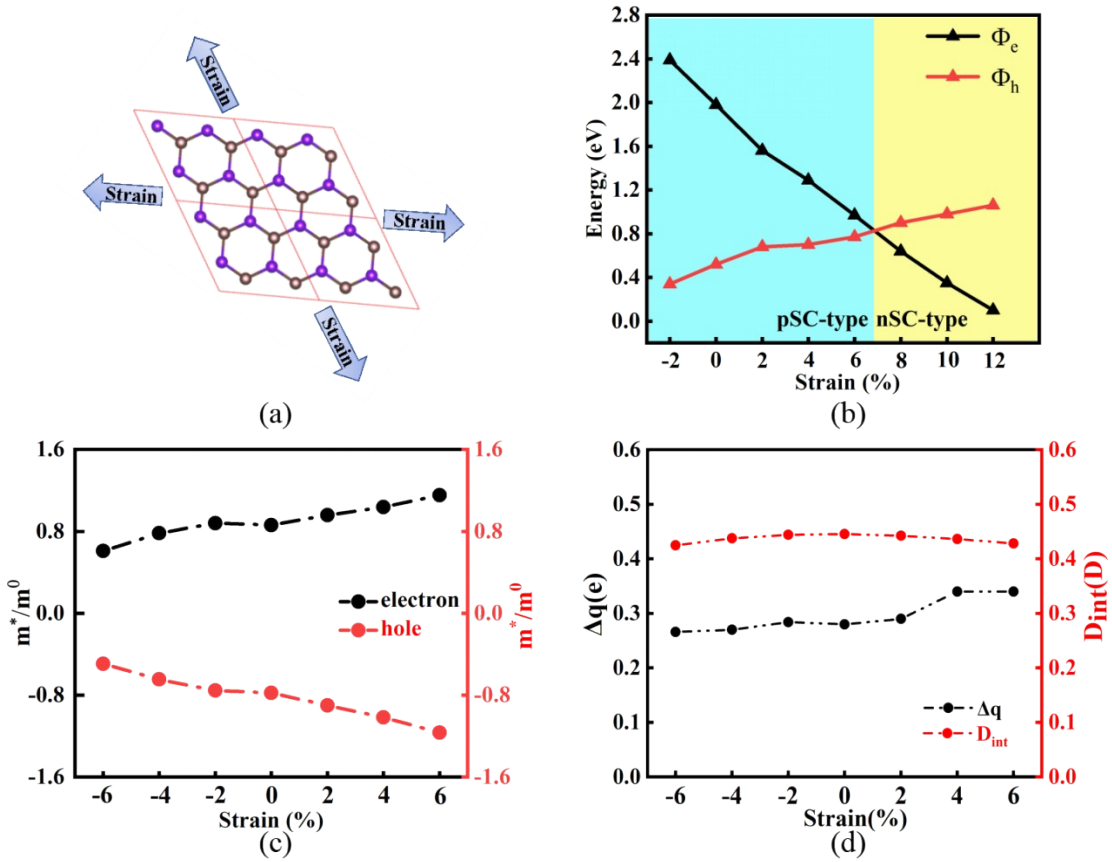

Fig. S6 The electronic properties of Ge/$(GaAs)_{As}$ heterostructure under different biaxial strain (a) The diagram of tensile biaxial strain, (b) The SBH for electron (Φ_e) and hole (Φ_h), (c) The effective masses of electrons and holes, (d) The charge transfer (Δq) and interfacial dipole moment (D_{int}).

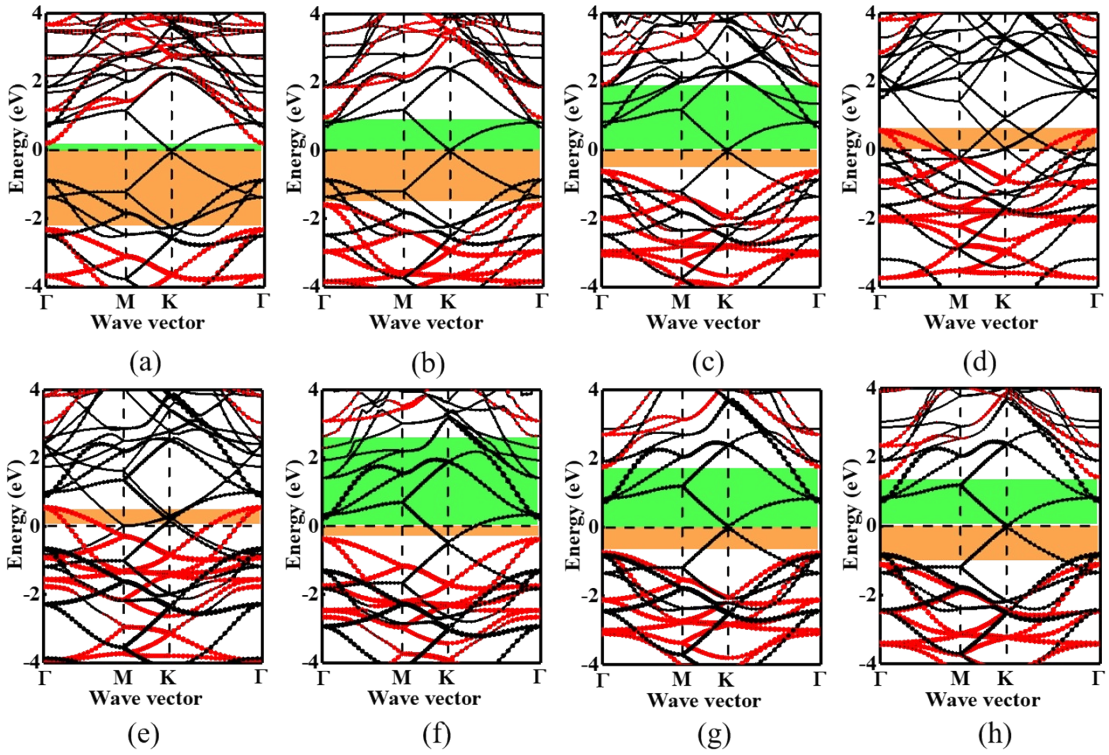

Fig. S7 The band structure of Ge/$(GaAs)_{Ga}$ under (a) -0.2 (V/Å), (b) 0 (V/Å), (c) 0.4 (V/Å) , (d) 1 (V/Å) electric fields, of Ge/$(GaAs)_{As}$ under (e) -0.2 (V/Å), (f) 0 (V/Å), (g) 0.4 (V/Å) , (h) 1 (V/Å) electric fields. The light green and light brown areas indicate the Φ_e and Φ_h, respectively.

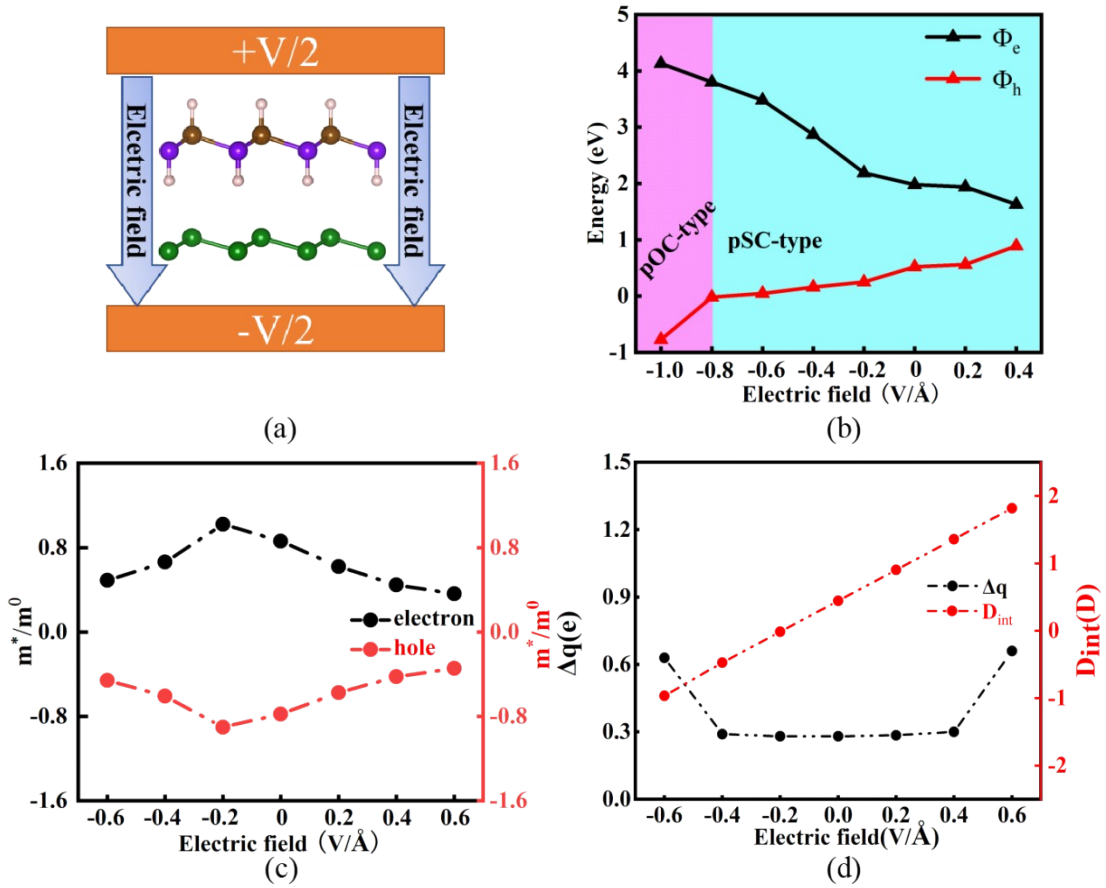

Fig. S8 The electronic properties of Ge/$(GaAs)_{As}$ heterostructure under different electric fields (a) The diagram of positive electric field, (b) The SBH for electron (Φ_e) and hole (Φ_h), (c) The effective masses of electrons and holes, (d)The charge transfer (Δq) and interfacial dipole moment (D_{int}).

Table S1 The computed tunneling barrier width (W_{TB}), tunneling barrier height (H_{TB}), and tunneling probability of carriers (P_{TB}) of Ge/GaAs heterostructure under different strain.

Ge/(GaAs)$_{Ga}$							
Strain (%)	-6	-4	-2	0	2	4	6
W_{TB} **(Å)**	2.81	2.85	2.89	2.90	2.95	2.96	2.97
H_{TB} **(eV)**	2.43	2.38	2.33	2.26	2.23	2.12	2.05
P_{TB} **(%)**	1.55	1.64	1.73	1.95	1.98	2.39	2.69
Ge/(GaAs)$_{As}$							
Strain (%)	-6	-4	-2	0	2	4	6
W_{TB} **(Å)**	1.37	1.42	1.51	1.53	1.46	1.53	1.54
H_{TB} **(eV)**	0.94	0.96	0.98	1.03	0.92	0.91	0.89
P_{TB} **(%)**	32.43	31.01	29.15	27.14	32.05	31.60	32.29

Table S2 The computed tunneling barrier width (W_{TB}), tunneling barrier height (H_{TB}), and tunneling probability of carriers (P_{TB}) of Ge/GaAs heterostructure under different electric field.

Ge/(GaAs)$_{Ga}$							
Electric field (V/Å)	-0.6	-0.4	-0.2	0	0.2	0.4	6
W_{TB} **(Å)**	2.39	2.84	2.87	2.90	2.91	2.93	2.94
H_{TB} **(eV)**	1.98	2.33	2.30	2.26	2.25	2.23	2.21
P_{TB} **(%)**	4.36	1.80	1.85	1.94	1.97	2.01	2.07
Ge/(GaAs)$_{Ga}$							
Electric field (V/Å)	-0.6	-0.4	-0.2	0	0.2	0.4	6
W_{TB} **(Å)**	1.67	1.63	1.55	1.53	1.49	1.48	1.50
H_{TB} **(eV)**	1.08	1.05	1.04	1.03	1.03	1.03	1.03
P_{TB} **(%)**	24.0	25.3	26.5	27.1	27.6	27.7	27.5